JOURNAL OF SOLID STATE CHEMISTRY 31, 171–188 (1980)

Phase Diagram and Some Physical Properties of V_2O_{3+x}* ($0 \leq x \leq 0.080$)

Y. UEDA, K. KOSUGE, AND S. KACHI

Department of Chemistry, Faculty of Science, Kyoto University, Kyoto, Japan

Received October 18, 1978; in revised form March 6, 1979

The magnetic and electric properties of V_2O_{3+x} were investigated by measurements of magnetic susceptibility, electrical resistivity, magnetotorque, Mössbauer of doped ^{57}Fe, and NMR of ^{51}V, and the results were compared with those of the $(V_{1-x}Ti_x)_2O_3$ system or highly pressured V_2O_3. The results obtained are as follows: (1) The metallic state shows an antiferromagnetic ordering at $T_N(x)$. The value of T_N for metallic V_2O_3, obtained by interpolation to $x = 0$, shows the coincidence between V_2O_{3+x} and the $(V_{1-x}Ti_x)_2O_3$ system. (2) Magnetic susceptibility of V_2O_{3+x} is expressed as $\chi_M(V_2O_{3+x}) = (1-x)\chi_M(V^{3+}) + x\chi_M(V^{4+})$. $\chi_M(V^{4+})$ obeys the Curie–Weiss law ($\chi_M(V^{4+}) = 0.77/T + 17$). (3) In the insulating phase, the electrical resistivity ρ is expressed as a common equation: $\rho = 10^{-1.8}\exp(E/kT)$. This implies that the substitution of Ti or nonstoichiometry (V^{+4} + metal vacancies) has little influence on the carrier mobility (or bandwidth). (4) There is a critical length in the c-axis ($\simeq$14.01 Å) where the metal–insulator transition takes place. This suggests that the length of the c-axis plays an important role in the metal–insulator transition of V_2O_3-related compounds.

1. Introduction

Vanadium sesquioxide (V_2O_3) shows a successive phase transition of insulator to metal to insulator. One is a sharp first-order transition from a high-temperature metallic, corundum phase to a low-temperature antiferromagnetic insulating, monoclinic phase at about 170°K (T_{t1}), accompanied by a change in resistivity of about 7 orders of magnitude and a reduction of magnetic susceptibility. The other[1] is a continuous change back to a paramagnetic insulating state at around 500°K (T_{t2}), showing an anomaly that is marked by continuous change of the lattice parameter, resistivity, and magnetic susceptibility.

The effect of various dopants such as Sc, Ti, Cr, Fe, Zr, Al, and Mg on these transitions has been extensively studied by Bell

* From the viewpoint of defect structure, the notation V_2O_{3+x} has to be changed to $V_{2-y}O_3$, because the nonstoichiometry in V_2O_3 originates from the metal vacancies. However, in this paper we use the notation V_2O_{3+x} for convenience.

[1] Much work has been done on the anomalous behavior of the electrical resistivity, magnetic susceptibility, and lattice constant appearing in V_2O_3 at around 500°K (T_{t2}). McWhan *et al.* (Ref. (*5*)) attributed it to the supercritical behavior and also claimed the material is insulating above T_{t2}. Honig's group (*Phys. Rev. Lett.* **32**, 13, 1974) reported that the material is a metal, a semimetal, or a degenerated-band semiconductor above T_{t2}. From a nuclear magnetic resonance study, Kerlin *et al.* (*Solid State Commun.* **13**, 1125, 1973) concluded that above T_{t2}, V_2O_3 is an insulator with localized magnetic moment. They showed that the observed relaxation rate below 320°K satisfies quite well the Korringa relation, a characteristic of metals, and above 550°K is constant as expected for a paramagnetic insulator. This behavior of the high-temperature relaxation rate directly reflects the localized character of the 3*d* electrons on every atomic site in the insulating phase. This NMR experiment is most persuasive to us, because NMR is one of the most powerful tools for examining the electronic state of materials. Therefore, we believe that above T_{t2}, V_2O_3 is an insulator with a local moment. It is to be noted that the purpose of paper is to make clear the PM–AFI transition of V_2O_3.

0022-4596/80/020171-18$02.00/0
Copyright © 1980 by Academic Press, Inc.
All rights of reproduction in any form reserved.
Printed in Great Britain

Laboratories (*1–3*). Their experiments on the mixed-oxide systems $(V_{1-x}Cr_x)_2O_3$ and $(V_{1-x}Ti_x)_2O_3$ as a function of temperature or pressure (*3–5*) have shown that these transitions can be regarded as a transition from a highly correlated metallic phase to a localized insulating phase, which was originally proposed by Mott (*6, 7*). The generalized phase diagram adopted from Ref. (*3*) is shown in Fig. 1. This phase diagram is constructed from three defined regions: paramagnetic metal (PM), paramagnetic insulator (PI), and antiferromagnetic insulator (AFI). The first-order PM–PI phase boundary is terminated at a critical point and the continuous change of V_2O_3 at around 500°K is due to supercritical behavior, being analogous to the solid–solid phase boundary in cerium metal (*8, 9*).

On the other hand, these phase transitions have been studied by controlling anion content (nonstoichiometric compounds) (*10–16*) or by substituting another anion such as fluorine for oxygen in V_2O_3 (*17*). As shown in the results, nonstoichiometry and the substitution of fluorine suppress the insulating phase.

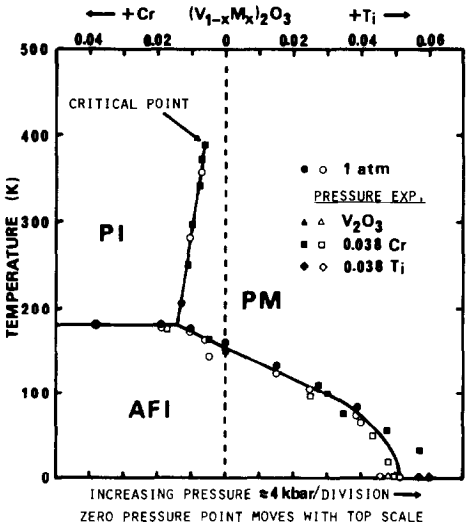

FIG. 1. Generalized phase diagram for the metal–insulator transition in V_2O_3 as a function of doping with Cr or Ti and as a function of pressure (Ref. (*3*)). The solid and open symbols represent increasing and decreasing pressure or temperature, respectively.

In the metallic phase, the magnetic susceptibility obeys the Curie–Weiss law with $C = 0.657$ (emu/mole) °K and $\Theta = 600$°K (*18*). It has been an interesting problem whether the metallic phase orders magnetically at lower temperatures. Unfortunately, the first-order transition of stoichiometric V_2O_3 occurs at T_{t1}. To stabilize the metallic phase, down to the lowest temperature, there are three methods, i.e., the substitution of Ti for V, excess oxygen (V_2O_{3+x}), and high pressure. The nuclear magnetic resonance (NMR) study on the pressure-stabilized metallic V_2O_3 (*19*) revealed that no magnetic ordering was observed down to 4.2°K, which suggests that the metallic state has no localized moment, in contrast to the paramagnetic insulating phase. Our recent studies on the nonstoichiometric V_2O_{3+x} (*16, 20*) confirmed that V_2O_{3+x} shows a paramagnetic metal (PM) to an antiferromagnetic metal (AFM) transition at about 10°K in the composition region $0.04 \leq x \leq 0.08$. The magnetic ordering of the metallic phase was also observed on the $(V_{1-x}Ti_x)_2O_3$ system by Dumas and Schlenker (*21*) and our group (*22*). These results are at variance with the reports of McWhan *et al.* (*3, 12*).

In this paper, we report the details of the magnetic and electric properties of the system V_2O_{3+x}. The comparison of the V_2O_{3+x} system with the $(V_{1-x}Ti_x)_2O_3$ system or the obtained phase diagram to the generalized phase diagram will be also discussed.

2. Experimental

The powder samples of V_2O_{3+x} were prepared by the ceramic method, i.e., the weighed mixtures of stoichiometric V_2O_3 and V_2O_5 were pressed into a pellet, heated for 2 days at 600°C, then for 3 days at 1300°C in an evacuated silica tube, and then quen-

ched in ice water. The stoichiometric V_2O_3 powder samples were prepared by reducing V_2O_5 in hydrogen gas at 800°C for 3 days. The obtained V_2O_3 samples have a high T_{t1} (about 170°K on heating). The oxygen content in V_2O_{3+x} was analyzed by oxidizing the sample to V_2O_5 in air at 600°C. The accuracy of this method was estimated to be ± 0.002 in x of V_2O_{3+x}. The lattice parameters at room temperature vs composition (x) curves were determined (see Fig. 2). These curves were used to determine the composition of the powder or single-crystal samples for which the physical properties were measured.

Single crystals of V_2O_3 were grown by the chemical transport method (*23*). The procedure was the same as that of the crystal growth experiments on V_6O_{13} reported in a previous paper (*24*); the temperature of the charge zone was 1000°C and that of growth zone was 950°C. Single crystals of V_2O_{3+x} were prepared by heating a small crystal of V_2O_3 embedded in a large quantity of the powder sample of V_2O_{3+x} in an evacuated silica tube at 1300°C for 3 days.

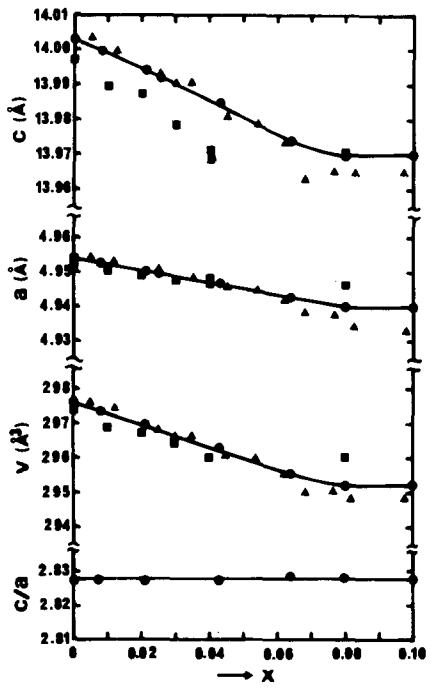

FIG. 2. Lattice parameters, volume, and c/a vs x in V_2O_{3+x} at room temperature. The circles are from the present work, triangles from Ref. (*11*), and squares from Ref. (*12*). A second-phase V_3O_5 starts to appear at $x > 0.08$ in the present work.

The samples $(V_{1-x}Ti_x)_2O_3$ $(0 \leq x \leq 0.3)$ were prepared by arc melting of an appropriate mixture of V_2O_3, Ti metal, and TiO_2.

The magnetic susceptibility measurement was made with a magnetic torsion balance. For the Mössbauer measurement, V_2O_{3+x} samples doped with 1% $^{57}Fe_2O_3$ were prepared by the ceramic method. The velocity scale in Mössbauer spectra was calibrated with pure Fe metal. Susceptibility curves of ^{57}Fe-doped samples showed that the effect of the impurity Fe on the intrinsic properties of V_2O_{3+x} is not so significant. The magneto-torque measurement was carried out with a torque magnetometer, using a single-crystal specimen of 10–20 mg. The magnetization measurement was made with a flux magnetometer using a 50-kOe superconductor magnet. The electric resistivity measurement was made by the ordinary four-probe method using single-crystal or sintered samples. The NMR measurement was made with an ordinary coherent or incoherent, high-power pulsed NMR spectrometer.

3. Results

3.1. Latttice Parameters

The lattice parameters obtained at room temperature vs composition (x) are shown in Fig. 2, including the data of Nakahira *et al.* (*11*) and McWhan *et al.* (*12*). Both the a-axis and c-axis of corundum structure show a smooth decrease up to $x = 0.080$ in V_2O_{3+x} and then become scarcely dependent on x, coinciding with the appearance of V_3O_5 as the second phase. This suggests that the limit of nonstoichiometry in the corundum phase is about $x = 0.080$. The dependence of the

lattice parameters on x is in good agreement with the findings of Nakahira *et al.* and McWhan *et al.*, although the limit of nonstoichiometry is different among the three works ($x \simeq 0.06$ for McWhan *et al.* and $x \simeq 0.10$ for Nakahira *et al.*); the discrepancy of the limit of x may be caused by the difference of the temperatures at which the samples were prepared.

The temperature dependence of the lattice parameters for the $x = 0.00$, 0.020, 0.045, and 0.062 single-crystal samples was measured in the temperature region from 77°K to room temperature. The results are shown in Fig. 3. The a-axis smoothly decreases with decreasing temperature and the c-axis linearly increases with decreasing temperature. The volume decreases with temperature. The samples of $x = 0.00$ and 0.020 show the metal–insulator transition and the samples of $x = 0.045$ and 0.062 are metallic down to absolute zero. For $x =$ 0.045, the c-axis, extrapolated to 4.2°K, coincides very well with the data of McWhan *et al.* (*25*) but the a-axis does not, as shown in Fig. 3.

3.2. Magnetic Susceptibility and Magnetization Measurements

The magnetic susceptibility (χ) was measured in the temperature range from 4.2 to 900°K. The results are shown in Figs. 4 and 5. The PM–AFI transition of V_2O_3 accompanies a reduction of χ at T_{t1}. As shown in Fig. 4, T_{t1} decreases with increasing x, and the samples with $x \geq 0.035$ do not show a PM–AFI transition. Above 80°K, the temperature dependence of χ in the nonstoichiometric V_2O_{3+x} is very similar to that of stoichiometric V_2O_3. Below this temperature, χ gradually deviates from the Curie–Weiss law and the deviation increases with increasing x. These results are in good agreement with those of McWhan *et al.* (*12*). It is to be noted that χ of the samples with $x \geq 0.035$ shows an anomaly at about 10°K,

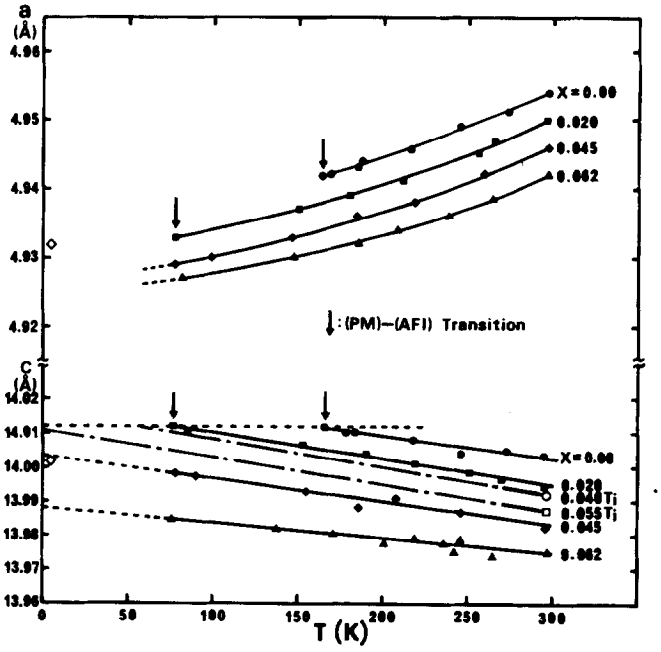

FIG. 3. Lattice parameters vs temperature for samples of V_2O_{3+x} in the temperature range from 77°K to room temperature. The solid symbols are from the present work, open symbols for $x = 0.045$ from Ref. (*25*) and for 4 and 5.5% Ti from Ref. (*3*).

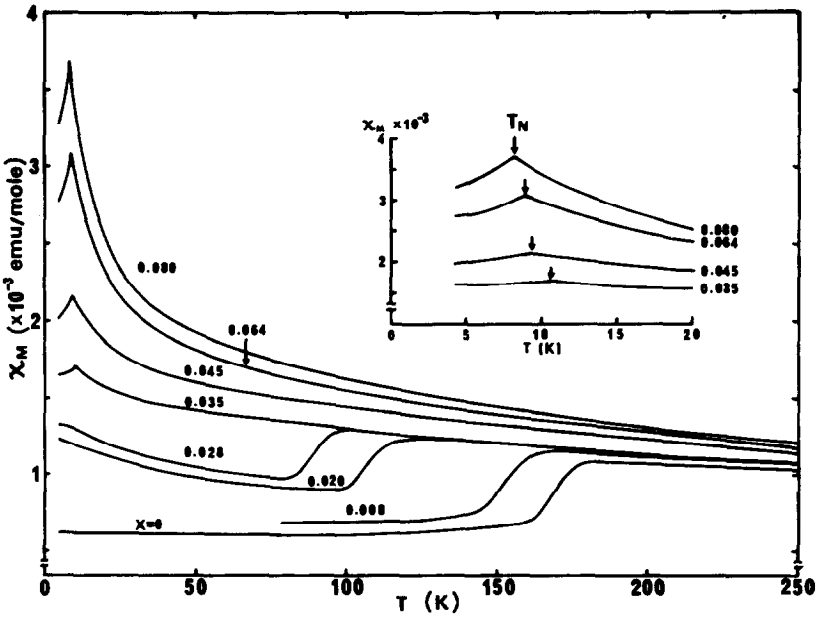

FIG. 4. Magnetic susceptibility vs temperature curves for V_2O_{3+x} below 250°K. The PM–AFI transition temperature shifts downward with increasing x and the samples with $x \geq 0.035$ do not show the transition. Note an anomaly at around 10°K (T_N) for the samples with $x \geq 0.035$. The inset shows the dependence of T_N on x. It was confirmed in Sect. 3 that this anomaly at T_N is caused by the antiferromagnetic ordering.

which suggests the antiferromagnetic ordering. The temperature at which χ shows an anomaly decreases slightly with increasing x, i.e., 11°K for $x = 0.035$ and 8°K for $x = 0.080$, as shown in the inset of Fig. 4.

On the other hand, the PM–PI transition of V_2O_3 at T_{t2} is characterized by a plateau in the χ vs T curve. As shown in Fig. 5, the temperature region (T_{t2}) in which the χ vs T curve shows a plateau becomes narrower and shifts toward higher temperature with increasing x up to about $x = 0.03$. In the samples with $0.040 \leq x \leq 0.080$, the χ vs T curves show no plateau and the PM–PI transition smears out.

The measurement of the magnetization for the sample with $x = 0.040$ was made in the field up to 50 kOe at 4.2 and 1.36°K. The magnetization (M) is proportional to the applied field (H) at both temperatures and shows the absence of any significant saturation. The slope (M/H) is slightly larger at 4.2°K than at 1.36°K. This is consistent with the behavior of χ measured with the magnetic torsion balance. These results suggest that the curves correspond to those in the antiferromagnetic regime.

3.3. *Mössbauer Effect Measurements*

Mössbauer effect measurements (*16*) were made for the purpose of confirming the magnetic ordering. The measurements were made on the ^{57}Fe-doped samples with $x = 0$, 0.02, 0.04, and 0.06 at 4.2°K, 77°K, and room temperature. The obtained results are summarized in Table I. At room temperature the Mössbauer spectrum of each sample is a single line, the isomer shift (IS) is about 0.65 mm/sec relative to pure Fe metal, and the linewidth is 0.4 mm/sec. The $x = 0$ and 0.02 samples show the PM–AFI transition and show magnetic hyperfine splitting below the transition temperature. The hyperfine field (Hi) for $x = 0.02$ at 4.2°K is 452 kOe

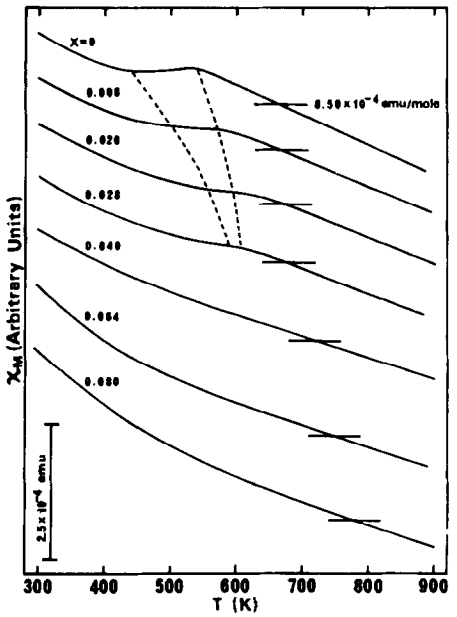

FIG. 5. Magnetic susceptibility vs temperature curves for V_2O_{3+x} above 300°K. The temperature interval of the PM–PI transition becomes narrower and shifts toward higher temperature with increasing x, as shown by the broken line. In the samples with $x \geq 0.04$, the PM–PI transition smears out.

and is nearly equal to that for stoichiometric V_2O_3. The IS of the AFI phase is about 0.63 mm/sec and a little smaller than that of the PM phase. The Mössbauer parameters for the AFI phase are reasonable as values for trivalent iron, although the hyperfine field is somewhat smaller than is typical.

TABLE I

MÖSSBAUER PARAMETERS

	T (°K)	H_i (kOe)	IS (mm/sec)
V_2O_3	300	para.	0.67 ± 0.03
	77	387 ± 2.5	0.64
	4.2	458	0.62
$V_2O_{3.02}$	4.2	452	0.63
$V_2O_{3.04}$	4.2	273	0.73
$V_2O_{3.06}$	300	para.	0.64
	77	para.	0.78
	4.2	263	0.73
	2	283	0.76

The $x = 0.04$ and 0.06 samples, which show no PM–AFI transition, are still paramagnetic at 77°K and show a smaller hyperfine field at 4.2°K. The hyperfine field for $x = 0.04$ at 4.2°K is 273 kOe and those for $x = 0.06$ at 4.2 and 2.0°K are 263 and 283 kOe, respectively. These results support the hypothesis that the anomaly of the susceptibility curves at about 10°K is caused by the magnetic ordering. The extrapolated hyperfine field to absolute zero is about 290 kOe, which is too small to regard as the field of a trivalent iron. The small hyperfine field and the large isomer shift, compared with that of the AFI phase, reflect the metallic properties of the matrix.

3.4. Magnetotorque Measurements

Magnetic anisotropy was measured by magnetotorque measurements. Torques under the various field intensities at 4.2°K, 77°K, and room temperature were measured both in the c plane (the plane perpendicular to c-axis) and in the c–a plane (the plane perpendicular to the c plane) of the single crystal of $V_2O_{3.080}$ which is metallic down to the lowest temperature. The torque curves in the c–a plane are shown in Fig. 6. The curves show twofold symmetry at all temperatures and the torque amplitudes are proportional to the square of the field strength (H), as shown in the inset of Fig. 6. Therefore, the torque T is given by the formula

$$T = \tfrac{1}{2}\Delta\chi H^2 \sin 2\Theta.$$

As shown in Fig. 6, the two principal axes in the c–a plane are the c-axis and the a-axis at all temperatures and therefore $\Delta\chi$ is $\chi_a - \chi_c$, where Θ is the angle of the direction of the applied field from the c-axis. The c-axis is the axis of difficult magnetization ($\Delta\chi = \chi_a - \chi_c > 0$) at 77 and 300°K, but the curve at 4.2°K changes the phase by 90° as compared with the curves at 77 and 300°K, i.e., the c-axis is the axis of easy magnetization ($\Delta\chi = \chi_a - \chi_c < 0$). Torque amplitude ($T_{max}$) at 4.2°K is much larger than at 77°K, suggesting that the increase of the magnetic anisotropy is due to antiferromagnetic ordering.

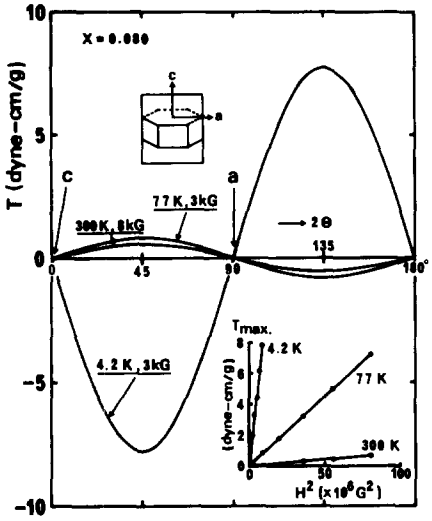

FIG. 6. Torque curves in the c–a plane for single-crystal $V_2O_{3.080}$. The principal axes are the a- and c-axis at all temperatures. The curve at 4.2°K has a large torque amplitude and changes phase by 90° compared with the curves at 77 and 300°K.

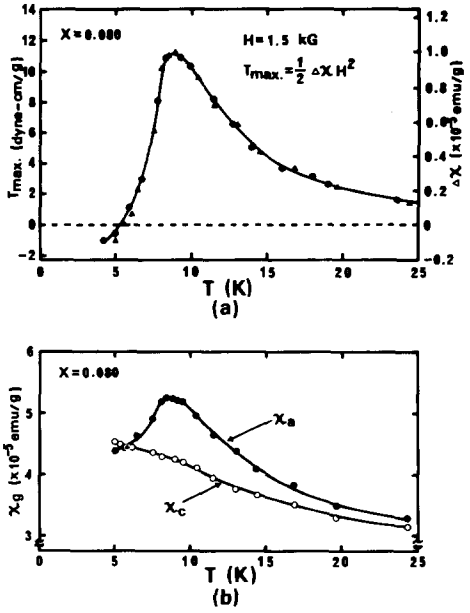

FIG. 7. (a) Temperature dependence of torque amplitude (T_{max}) at 1.5 kG and $\Delta\chi(=\chi_a-\chi_c)$. T_{max} and $\Delta\chi$ are combined by the equation $T_{max}=\frac{1}{2}\Delta\chi H^2$. The solid triangles are from the direct measurements of χ_a and χ_c. (b) Magnetic susceptibility along the a-axis and c-axis vs temperature curves for single-crystal $V_2O_{3.080}$.

On the other hand, the torques in the c plane were nearly zero at all temperatures, i.e., $\Delta\chi=0$. This reflects the symmetry of crystal structure (hexagonal) in the paramagnetic state. In the antiferromagnetic state, it is regarded that the direction of antiferromagnetic spin is in the direction of the difficult axis. From the results that the difficult axis is the a-axis at 4.2°K, it is confirmed that the direction of the antiferromagnetic spin axis is in the c plane. The result that the torques in the c plane are nearly zero suggests that the three magnetic domains exist in the c plane and are caused by the crystal structure (hexagonal symmetry).

Figure 7a shows the temperature dependence of the torque amplitude (T_{max}). T_{max} sharply increases with increasing temperature and afterward smoothly decreases with increasing temperature, showing a maximum at around 8°K. T_{max} is related with $\Delta\chi$ by the formula $\Delta\chi=2T_{max}/H^2$, where $\Delta\chi$ is $\chi_a-\chi_c$. Figure 7b shows χ_a and χ_c vs temperature curves, directly measured using a single crystal of $V_2O_{3.080}$ with magnetic torsion balance. The obtained temperature dependence of $\Delta\chi(=\chi_a-\chi_c)$ is in good agreement with the results from T_{max}, as shown by the solid triangles in Fig. 7a. From the temperature dependence of T_{max} and the directly measured χ_a and χ_c, it is confirmed that the Néel temperature, T_N, is about 8°K in $V_2O_{3.080}$.

3.5. *NMR Measurements*

The above-mentioned experiments are somewhat macroscopic, so we studied ^{51}V NMR of nonstoichiometric V_2O_{3+x}. A part of the results has been already reported (*20*). We have observed two signals in the samples with $x=0.04$ and 0.06 at 1.8°K. One is the zero-field spin-echo signal distributed around 64 MHz and the hyperfine field is estimated to be 58 ± 2 kOe. The other is the broad spectrum obtained by sweeping the external field at constant frequency, and this spectrum may be interpreted as due to the

interplay of the external field and the hyperfine field, both being nearly the same magnitude, in the randomly oriented antiferromagnetic powder sample. The estimated hyperfine field is about 9 kOe. These signals were assigned for the former to be due to the V^{4+}-like sites, associated with the charge compensation caused by nonstoichiometry, and for the latter to be due to the matrix V sites, respectively. From these results, it is directly proved that the metallic V_2O_{3+x} orders antiferromagnetically at lower temperature.

On the other hand, the spectra with strong intensity centered at 207 MHz and very weak intensity distributed around 79 MHz were observed at 1.8°K in the samples with $x = 0.01$ and 0.02, which show the PM–AFI transition. The estimated hyperfine fields for these spectra are 184.9 ± 0.5 and 71 ± 1 kOe, respectively. The former is almost equal to the hyperfine field (185.0 ± 0.1 kOe) found in the AFI phase of V_2O_3. The weak spectra may be due to V^{4+} sites and the hyperfine field is nearly the same as that (about 80 kOe) of V^{4+} in Magnéli phase oxides V_nO_{2n-1} (*26, 27*). This shows that in the AFI phase of V_2O_{3+x} the matrix V sites have the same electronic state as in the AFI phase of stoichiometric V_2O_3, and V^{4+} sites are localized in the matrix, having nearly the same magnetic properties as that of other insulating vanadium oxides. A detailed NMR study on the metallic V_2O_{3+x} is now in progress and will be reported elsewhere.

3.6. Electrical Resistivity Measurements

Electrical resistivity measurements of V_2O_{3+x} were made on single crystals or sintered samples in the temperature range from 1.8°K to room temperature. The results of single crystals on cooling are shown in Fig. 8a. The samples with $x = 0$, 0.017, and 0.028 show a PM–AFI transition at T_{t1} with a resistivity change of the order $\sim 10^7$. The samples with 0.040 and 0.062 are metallic in the temperature region $1.8 \sim 300$°K. Within

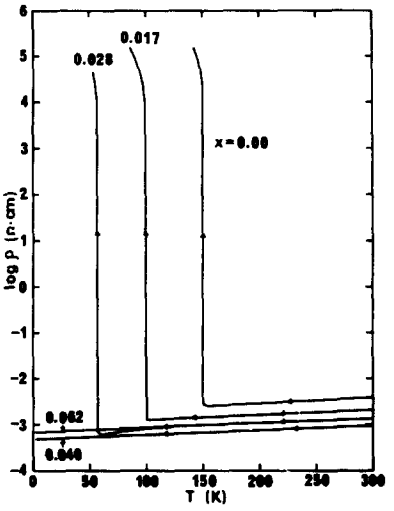

FIG. 8a. Resistivity vs temperature curves for single crystals of V_2O_{3+x} on cooling.

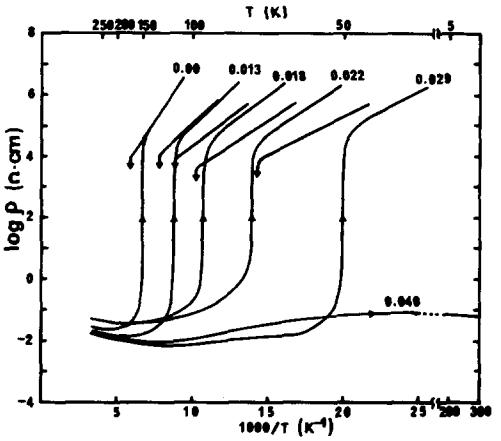

FIG. 8b. Resistivity vs reciprocal temperature for sintered samples of V_2O_{3+x}. The PM–AFI transition is suppressed with increasing x, showing a hysteresis by about 20°C between cooling and heating. The samples for $x \geq 0.040$ remain metallic down to absolute zero. The resistivity of the metallic phase of sintered samples is higher by $10^{1\sim2}$ orders than that of single crystals, probably caused by the grain boundary effect.

the experimental error, the value of resistivity ($\sim 10^{-3}\ \Omega \cdot$ cm) in the metallic state hardly depends on the nonstoichiometry. The resistivity measurement of the AFI phase was unsuccessful due to the breaking of the crystals through the PM–AFI transition but was performed successfully in

sintered samples. The results are shown as a plot of $\log\rho$ vs $10^3/T$ in Fig. 8b. In the sintered samples, the resistivity of the metallic phase is higher by $10^{1\sim2}$ orders than that in single crystals, and therefore the resistivity change at T_{t1} is smaller than that in single crystals. This might be caused by the grain boundary effect of sintered samples. The value of resistivity in the insulating phase is in good agreement with that of single crystals. Composition dependence of T_{t1}, activation energy (E_a) for resistivity in the AFI phase, and magnitude [2]($\Delta\rho$) of the discontinuity in resistivity at T_{t1} are shown in Fig. 9. T_{t1} shifts downward with increasing x, showing a hysteresis by about 20°C between cooling and heating. At $x \geq 0.04$, the AFI phase disappears and the system remains entirely metallic. E_a estimated from the slope of a plot of log ρ vs $10^3/T$ decreases with increasing x from about 0.15 eV at $x=0$ to 0.04 eV at $x \simeq 0.03$. Thereafter, E_a falls abruptly to zero at $x \simeq 0.033$. $\Delta\rho$ is scarcely dependent on x and is about 7 orders of magnitude. The dependence of T_{t1} on nonstoichiometry is in good agreement with the work of McWhan *et al.* (*12*).

The resistivity of the metallic phase for the samples with $x=0.040$ and 0.062 as a function of temperature is shown in Fig. 10. In both samples, the resistivity decreases almost linearly down to 130 ~ 150°K and more quickly below this temperature. The temperature dependence of the resistivity below about 130°K shows a $T^{1.4}$ dependence for $x=0.040$ and a $T^{1.2}$ dependence for $x=0.062$, as shown in Fig. 10. The resistivity of

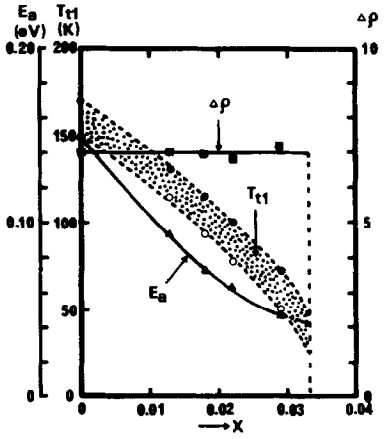

FIG. 9. Plot of metal–insulator transition temperature (T_{t1}), activation energy (E_a), and discontinuity in resistivity ($\Delta\rho$) vs composition (x) for sintered samples. The shaded region of T_{t1} shows a hysteresis between cooling and heating.

[2] $\Delta\rho$ is defined as $\Delta\rho = \log\rho_{T_{t1}} - \log 10^{-3}$, where $\rho_{T_{t1}}$ is the resistivity for sintered samples just below T_{t1}.

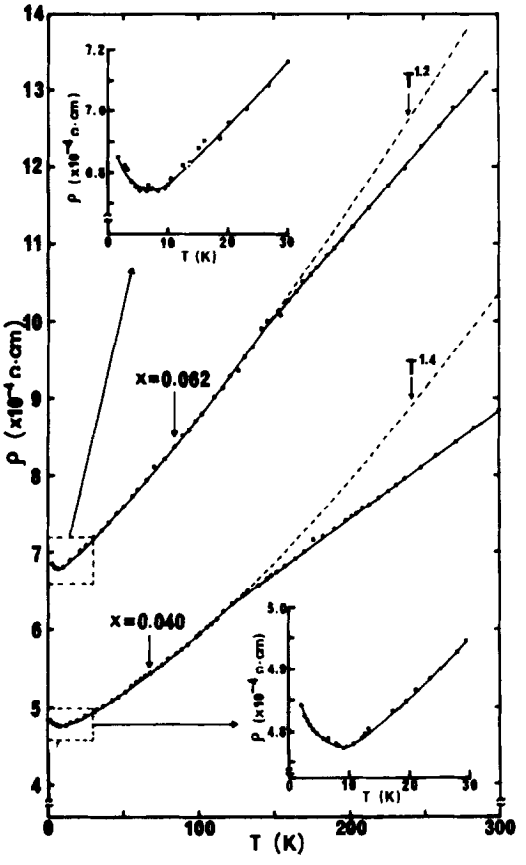

FIG. 10. Resistivity vs temperature for the samples with $x=0.040$ and 0.062 in V_2O_{3+x}. Both samples are metallic down to the lowest temperature. The resistivities for $x=0.040$ and 0.062 show $T^{1.4}$ and $T^{1.2}$ dependence at lower temperature, respectively. The insets show the temperature dependence of the resistivity in both samples below 30°K. Note that the resistivity shows a minimum at 8 ~ 10°K, corresponding to T_N.

metallic nonstoichiometric V_2O_{3+x} shows no T^2 dependence of the resistivity, which was observed in the metallic V_2O_3 stabilized by high pressure (*28*). It is noted that the resistivity of the samples with $x = 0.040$ and 0.062 shows a minimum at $8 \sim 10$°K, corresponding to T_N, as shown in the inset of Fig. 10.

3.7. Phase Diagram

The phase diagram of the V_2O_{3+x} system, obtained from the above-mentioned experimental results, is shown in Fig. 11. The PM–AFI transition shows a hysteresis on cooling and heating, and the line of T_{t1} in Fig. 11 was obtained from the intermediate value. The AFI phase is suppressed with increasing x and disappears at $x \geq 0.035$. On the other hand, the temperature interval, where the PM to PI phase transition takes place gradually, becomes narrower and shifts toward higher temperatures with x up to approximately $x = 0.03$, and the transition smears out at $x \geq 0.04$. At $x \geq 0.035$, the system remains entirely metallic and shows a transition from paramagnetic to antiferromagnetic at lower temperature. The transition temperature T_N slightly decreases with increasing x (11°K for $x = 0.035$ and 8°K for $x = 0.080$), as shown in the inset of Fig. 11. At $x > 0.080$, the V_3O_5 phase appears as the second phase.

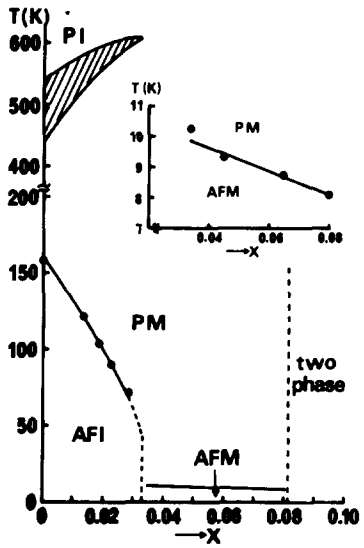

FIG. 11. Phase diagram of V_2O_{3+x}, obtained from experimental results.

4. Discussion

4.1. Magnetic Properties

χ obeys the Curie–Weiss law with $C = 0.657$ (emu/mole)°K and $\Theta = 600$°K in the metallic phase of V_2O_3 (*18*). The value of C is reasonable for V^{3+}, i.e., $3d^2$ state. If there were local moments in the metallic phase, they should have ordered magnetically at low temperature. The results of nuclear magnetic resonance under high pressure at 4.2°K, however, did not show any magnetic ordering (*19*). From the results, it was concluded that the metallic state has no localized magnetic moment, in contrast to the PI phase, and the observed temperature dependence of the susceptibility must be related to strongly interacting but still itinerant electrons.

In the V_2O_{3+x} system, the value of χ increases with x and the temperature dependence of χ is very similar to that of the stoichiometric V_2O_3 above 80°K. Below this temperature, χ gradually deviates from the Curie–Weiss law and the deviation increases with x. This result suggests that the molar susceptibility of V_2O_{3+x} consists of the matrix component and the excess component. On the basis of the ionic model, V_2O_{3+x} can be regarded as a mixed valence oxide consisting of $100(1-x)\%$ V^{3+}(matrix) and $100x\%$ V^{4+}. Therefore, it may be reasonable to conclude that the matrix component is due to $100(1-x)\%$ V^{3+} and the excess component is due to $100x\%$ V^{4+}. Then, the molar magnetic susceptibility ($\chi_M^{x_i}$) of $V_2O_{3+x_i}$ may be expressed as follows:

$$\chi_M^{x_i} = x_i\chi_M(V^{4+}) + (1-x_i)\chi_M(V^{3+}), \quad (1)$$

where $\chi_M(V^{4+})$ and $\chi_M(V^{3+})$ are the molar

susceptibilities related to V^{4+} and V^{3+} (matrix), respectively. We tried to estimate the magnetic susceptibility $\chi_M(V^{4+})$ by the following procedure. From Eq. (1), we have:

$$\frac{1}{1-x_i}\chi_M^{x_i} = \frac{x_i}{1-x_i}\chi_M(V^{4+}) + \chi_M(V^{3+}). \tag{2}$$

Therefore

$$\Delta\chi^{x_{ij}} = \frac{1}{1-x_i}\chi_M^{x_i} - \frac{1}{1-x_j}\chi_M^{x_j} = \left(\frac{x_i}{1-x_i} - \frac{x_j}{1-x_j}\right)\chi_M(V^{4+}), \tag{3}$$

$$\chi_M(V^{4+}) = \frac{(1-x_i)(1-x_j)}{x_i - x_j} \times \Delta\chi^{x_{ij}}, \tag{4}$$

$\chi_M(V^{4+})$ calculated from Eq. (4) has almost same value between different compositions and two examples of $\chi_M(V^{4+})$ and the inverse vs temperature curves are shown in Fig. 12a. The obtained $\chi_M(V^{4+})$ obeys a Curie–Weiss law: $\chi_M(V^{4+}) = 0.77/T + 17$ (emu/mole). The Curie constant is much larger than C calculated for V^{4+}, i.e., $S = \frac{1}{2}$ and is nearly equal to C of the metallic state of V_2O_3. The results of the NMR study suggest that V^{4+} ions in metallic V_2O_{3+x} behave as a localized impurity, having magnetic moment. The metallic phase of V_2O_3 is regarded as a system having a strong electron correlation and χ apparently obeys the Curie–Weiss law with $C = 0.657$ (emu/mole)°K. Therefore, V^{4+} ions are a rather localized impurity but C of impurity V^{4+} may be enhanced by the strong electron correlation.

Let us calculate $\chi_M(V^{3+})$ by use of the obtained $\chi_M(V^{4+})$ and Eq. (2). The result is shown in Fig. 12b as a function of temperature. The obtained $\chi_M(V^{3+})$ shows a good agreement with the observed χ_M for V_2O_3 of the metallic phase.

Thus, it can be concluded that the magnetic susceptibility of V_2O_{3+x} consists of the V^{4+}-like site component and the matrix component, and the matrix component has the same magnetic properties as the metallic phase of V_2O_3, which is consistent with the NMR results (*20*). As V_2O_3 transforms from metallic to insulating state at about 170°K, the temperature dependence of $\chi_M(V_2O_3)$ at lower temperature cannot be measured. The obtained temperature dependence of $\chi_M(V^{3+})$ may predict that of the magnetic susceptibility of metallic V_2O_3 down to the lowest temperature. The most interesting result is that $\chi_M(V^{3+})$ decreases with decreasing temperature below about 80°K in spite of the absence of the magnetic ordering. The temperature dependence of the ^{51}V Knight shift corresponds to that of magnetic susceptibility, and therefore a NMR study of the majority sites of the metallic V_2O_{3+x} at low temperature is now in progress.

On the other hand, the addition of Ti also stabilizes the metallic phase. χ vs T curves of the $(V_{1-x}Ti_x)_2O_3$ system measured for comparison are shown in Fig. 13. In this case, the deviation from the Curie–Weiss law with increasing x at lower temperature was not observed and χ slightly decreases with increasing x, in contrast to the V_2O_{3+x} system. Ti^{3+} has the same electronic state ($3d^1$) as V^{4+}. If the titanium enters as the localized impurity Ti^{3+} in the matrix, the same effect as that caused by V^{4+} is expected in the magnetic susceptibility. So Ti^{3+} is regarded as a delocalized impurity. McWhan *et al.* proposed that Ti^{3+} adds a slightly larger e^T orbital (*29*) to the matrix band and therefore causes an increase in the bandwidth, in contrast to the case of Cr^{3+} addition (*3*). The decrease of χ with increasing Ti concentration may be related to the increase of the bandwidth.

Thus, not only from NMR but also from the magnetic susceptibility measurements, it was concluded that in V_2O_{3+x} the V^{4+} sites behave like rather localized ions. On the other hand, Ti ions in the $(V_{1-x}Ti_x)_2O_3$ system have a delocalized character, which may contribute to the stabilization of the metallic phase.

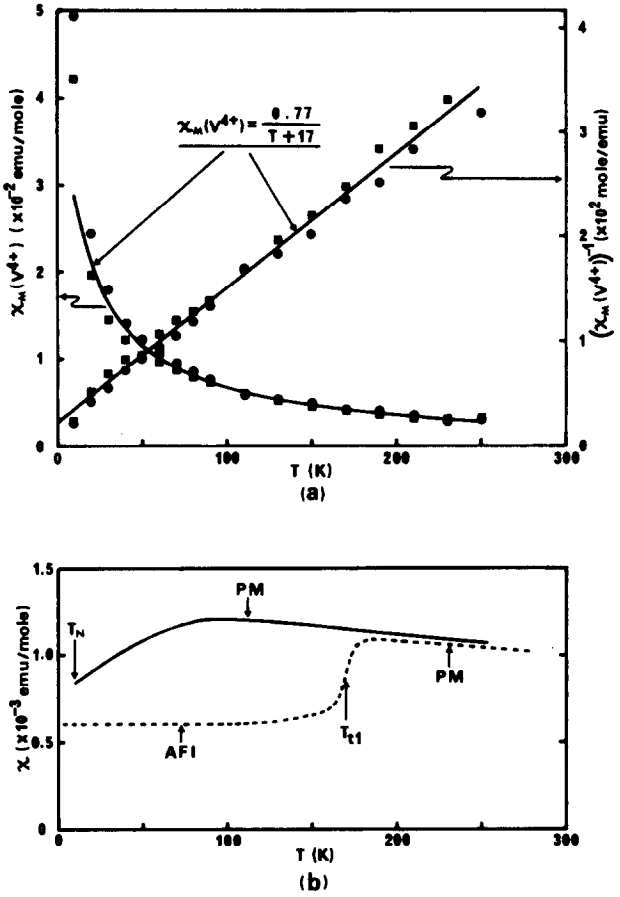

FIG. 12. (a) Magnetic susceptibility $\chi_M(V^{4+})$ and the inverse vs temperature in the V_2O_{3+x} system (see text). The solid circles are from $x_i = 0.064$ and $x_j = 0.045$, and the solid squares from $x_i = 0.080$ and $x_j = 0.045$ in Eq. (4). $\chi_M(V^{4+})$ obeys a Curie–Weiss law: $\chi_M(V^{4+}) = 0.77/T + 17$. (b) Magnetic susceptibility $\chi_M(V^{3+})$ vs temperature in the V_2O_{3+x} system. The solid line shows the temperature dependence of $\chi_M(V^{3+})$ calculated using $\chi_M(V^{4+})$ and Eq. (2). The broken line shows the temperature dependence of the magnetic susceptibility of stoichiometric V_2O_3. The calculated $\chi_M(V^{3+})$ shows a good agreement with the observed χ_M for V_2O_3 of the metallic phase. Note that $\chi_M(V^{3+})$ decreases with decreasing temperature below about 80°K, in spite of the absence of the magnetic ordering.

4.2. Electric Properties

It is well known that the impurity Cr^{3+} stabilizes the insulating phase of V_2O_3. The addition of Cr^{3+} causes a remarkable rise in the resistivity of the metallic phase. Meanwhile nonstoichiometry and the substitution of Ti for V stabilize the metallic phase, but the resistivity of the metallic phase is little affected. Figure 14 shows the comparison of E_a and $\Delta\rho$ of V_2O_{3+x} with those of $(V_{1-x}Ti_x)_2O_3$ reported by Kuwamoto *et al.* (*30*). In both systems, T_{t1} shifts downward with increasing x, and then there is an abrupt drop-off to 0°K as x passes the critical composition x_c above which the alloy system remains entirely metallic, where x_c is about 0.033 for V_2O_{3+x} and 0.055 for $(V_{1-x}Ti_x)_2O_3$. E_a diminishes from 0.15 eV to 0.04 eV smoothly and falls abruptly to zero at $x = x_c$ in V_2O_{3+x}, and in the $(V_{1-x}Ti_x)_2O_3$ system E_a approaches zero asymptotically at

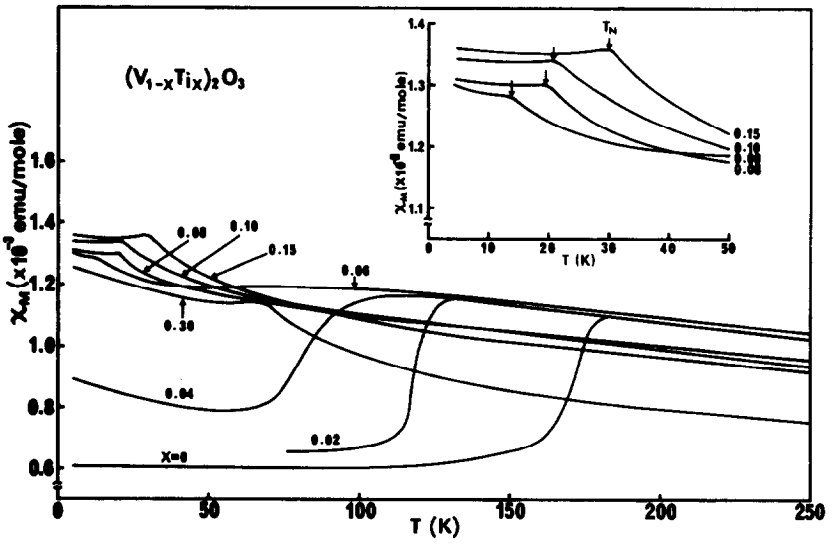

FIG. 13. Magnetic susceptibility vs temperature curves for the $(V_{1-x}Ti_x)_2O_3$ system ($0 \leq x \leq 0.30$). The magnetic susceptibility does not show the excess magnetic susceptibility, in contrast to the V_2O_{3+x} system.

$T_{t1} \to 0$. In the V_2O_{3+x} system $\Delta\rho$ is almost independent of x ($\Delta\rho \simeq 7$ orders of magnitude) and thereafter falls abruptly to zero at $x = x_c$. In the $(V_{1-x}Ti_x)_2O_3$ system $\Delta\rho$ decreases from 7 to 1.5 orders of magnitude with increasing x. The most significant difference between both systems is the x dependence of $\Delta\rho$.

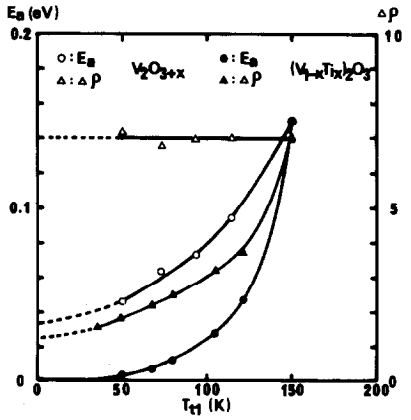

FIG. 14. Comparison of activation energy (E_a) and discontinuity in resistivity ($\Delta\rho$) vs transition temperature (T_{t1}) for the systems V_2O_{3+x} and $(V_{1-x}Ti_x)_2O_3$. It is to be noticed that the composition x in V_2O_{3+x} or $(V_{1-x}Ti_x)_2O_3$ is implicitly expressed by T_{t1}. The open symbols represent V_2O_{3+x} from the present work and the solid symbols $(V_{1-x}Ti_x)_2O_3$ from Ref. (*30*). The most significant difference between both systems is that $\Delta\rho$ is almost independent of T_{t1}, i.e., x, in the V_2O_{3+x} system and decreases with decreasing T_{t1} in the $(V_{1-x}Ti_x)_2O_3$ system.

Figure 15 shows a plot of $\log \rho_{T_{t1}}$ (resistivity just below T_{t1}) versus E_a/kT_{t1} for both systems. All measured points are scattered on the line for which the slope ($\log \rho/E_a/kT_{t1}$) is $\approx 1/2.3$. This implies that the temperature dependence of resistivity of both systems in the insulating phase is expressed as a common equation: $\rho = \rho_0 \exp E_a/kT$, where ρ_0 is $10^{-1.8}\ \Omega \cdot$ cm. In general, the electrical conductivity $\sigma(=1/\rho)$ is proportional to carrier concentration n and carrier mobility μ, i.e., $\rho = n\mu e$ (e, electron charge). For the case of the semiconductor, $n \propto \exp -E_a/kT$. In our case, ρ_0 is common for both systems, as mentioned above. This means that both the nonstoichiometry and the substitution of Ti for V do not affect the carrier mobility of the insulating phase, i.e., band structure or bandwidth. In the system $(V_{1-x}Ti_x)_2O_3$, the composition dependence of $\Delta\rho$ is fully explained by the dependence of the value E_a/kT_{t1} on the composition. In this case, the values of

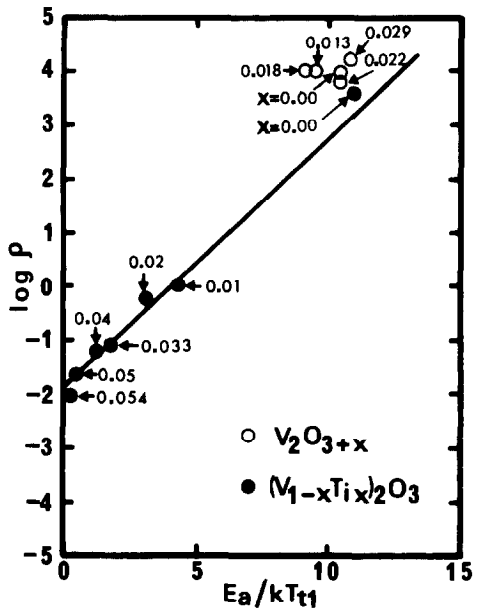

FIG. 15. Resistivity of the AFI phase at T_{t1} vs E_a/kT_{t1} for the V_2O_{3+x} and $(V_{1-x}Ti_x)_2O_3$ systems. The open circles represent the V_2O_{3+x} system and solid circles the $(V_{1-x}Ti_x)_2O_3$ system. The numerals show the composition x in V_2O_{3+x} or $(V_{1-x}Ti_x)_2O_3$. The solid line shows $\rho = 10^{-1.8}\exp(E_a/kT_{t1})$. All measured points are scattered on the solid line. This implies that the temperature dependence of resistivity of both systems in the AFI phase is expressed as a common equation: $\rho = 10^{-1.8}\exp(E_a/kT)$.

E_a/kT_{t1} decrease with increasing x. In the case of V_2O_{3+x}, the values of $\Delta\rho$ hardly depend on the composition, reflecting that the values of E_a/kT_{t1} are almost constant ($\simeq 10$). It is not clear why E_a/kT_{t1} is constant in the V_2O_{3+x} system and is changeable in the $(V_{1-x}Ti_x)_2O_3$ system. The estimated $\rho_0(\simeq 10^{-1.8}\,\Omega\cdot\text{cm})$ by the interpolation to $E_a/kT_{t1} = 0$ is larger by about 1 order than the resistivity (−3 orders) of the metallic phase. This suggests that the metallic state realized by $E_a = 0$ in the AFI phase is different from the metallic state of the PM phase intrinsically and therefore the PM–AFI transition is first order.

McWhan *et al.* proposed a large T^2 term as a significant character of the metallic phase of V_2O_3 from the resistivity measurements of high-pressure stabilized metallic V_2O_3 (*28*). In the system V_2O_{3+x}, the metallic V_2O_{3+x} shows no T^2 dependence of resistivity and the temperature dependence of the resistivity at low temperature can be fitted to $T^{1.4}$ (for $x = 0.040$) or $T^{1.2}$ (for $x = 0.062$) dependence rather than T^2, as shown in Fig. 10. This $T^{1.2\sim1.4}$ dependence of resistivity saturates at $100 \sim 150$°K. We have no proper theory which explains such a $T^{1.2\sim1.4}$ dependence. This behavior may be also related to the highly correlated electrons. The resistivity of metallic V_2O_{3+x} shows a minimum at about 8°K, as shown in the inset of Fig. 10. The minimum of resistivity is probably caused by the magnetic ordering.

4.3. The Metallic Antiferromagnetism

McWhan *et al.* measured the low-temperature heat capacity of metallic $V_{1.97}O_3$ ($V_2O_{3.046}$) several years ago (*25*). In this study, they observed the large linear term (γ) of the heat capacity and the excess heat capacity (ΔC_p^{ex}) above that calculated from $\gamma T + \beta T^3$. The origin of the excess heat capacity was concluded to come from a transition of an impurity phase and not from intrinsic properties of the materials. The temperature at which the excess heat capacity shows a peak is in good agreement with T_N observed in the nonstoichiometric metallic V_2O_{3+x} (see Fig. 4 in Ref. (*25*)). Accordingly, it can be deduced that the origin of ΔC_p^{ex} comes from the magnetic transition. As the majority of V sites are almost completely delocalized judging from the results of NMR measurements, the contribution of the majority sites to the heat capacity due to the magnetic entropy change can be estimated to be very small. Therefore, the observed excess heat capacity is regarded as the heat capacity due to the magnetic ordering of V^{4+}-like sites. If the V^{4+}-like sites are completely localized, the magnetic entropy change caused by the magnetic ordering is estimated to be $\Delta S = R\ \ln(2S+1) = 0.046 \times 1.38 = 0.063$ cal/°K

with $S=\frac{1}{2}$, taking the proportion of V^{4+} into consideration. ΔS calculated from Fig. 4 in Ref. (*25*) is about 0.015 cal/°K and smaller than that estimated as $S=\frac{1}{2}$. However, this value may be reasonable, considering the greater delocalization of the moments in the minority sites of the AFM phase (*20*).

The existence of the AFM phase was confirmed in this study. Our main interest is the magnetism of the majority V sites. The very small hyperfine field (9 kOe) of the majority sites is considered to be due to either the transferred hyperfine field from the localized V^{4+}-like sites or the contact hyperfine field associated with the *d*-spin polarization of the majority V sites. If the former is the case, only the V^{4+}-like sites with low concentration order magnetically in the nonmagnetic metallic matrix. This feature may belong to the spin-glass regime. However, the metallic antiferromagnetism observed in the nonstoichiometric V_2O_{3+x} does not show any of the characteristics of the spin-glass.[3] If the latter is the case, the magnetically ordered state can be regarded as an itinerant antiferromagnetism.

Recently, it was confirmed by Dumas and Schlenker (*21*) and then us (*22*) that the metallic phase stabilized by the substitution of Ti for V also shows the antiferromagnetic ordering. In this system, the magnetic susceptibility does not show the excess magnetic susceptibility, in contrast to the system V_2O_{3+x}, as shown in Fig. 13. Whether the observed AFM phase in both systems is induced by extrinsic condition (the addition of Ti or nonstoichiometry) or is intrinsic in V_2O_3 is an interesting problem. The interpolated T_N (~10°K) to $x=0$ in the V_2O_{3+x} system is in good agreement with that (see Fig. 1 in Ref. (*22*)) in the $(V_{1-x}Ti_x)_2O_3$ system. This suggests strongly that the metallic phase of stoichiometric V_2O_3 orders antiferromagnetically if the metallic phase is stable down to the lowest temperature.[4]

4.4. The Metal–Insulator Transition

The doping experiments of various cations such as Sc, Ti, Cr, Fe, Zr, Al, and Mg or the study of nonstoichiometric V_2O_{3+x} confirmed that only two cases, i.e., the substitution of Ti for V and the nonstoichiometry, stabilize the metallic phase down to the lowest temperature and the other dopants stabilize the insulating phase. These results suggest that the valence and ionic size of the impurity and electron concentration are not such significant controlling factors on the metal–insulator transition. Figure 1 shows that there is an empirical scaling between the addition of Cr^{3+} or Ti^{3+} and the pressure (negative and positive, respectively). This type of phase diagram as a function of pressure was originally proposed by Mott. McWhan *et al.* proposed that the PM–PI transition is an example of a Mott transition, that is, the highly correlated metallic state transforms to an insulating state in which electron correlation plays a dominant role, as in Mott–Hubbard insulators, by further dilating the lattice due to the addition of Cr (*2–4*).

We shall discuss the PM–AFI transition on the three cases in which the metallic phase is stabilized, i.e., (1) highly pressured V_2O_3, (2) the $(V_{1-x}Ti_x)_2O_3$ system, and (3) the V_2O_{3+x} system. The dependence of the lattice parameters for these three samples at room temperature on the composition x or

[3] For example, the sharpness of the anomaly of magnetic susceptibility at T_f (freezing temperature) depends on the external field in many spin-glass materials but does not in the case of V_2O_{3+x}, and T_f roughly shows a linear concentration dependence in the spin-glass regime but T_N for V_2O_{3+x} slightly decreases with increasing of V^{4+} concentration (x). Therefore, we concluded that the AFM phase of the V_2O_{3+x} system does not deal with a spin-glass.

[4] This seems to be somewhat inconsistent with the data of Gossard *et al.* (Ref. (*19*)). They confirmed by NMR study that the pressure-stabilized metallic phase of V_2O_3 does not order magnetically down to 4.2°K. However, it may be possible that the Néel temperature is suppressed below 4.2°K by high pressure (>26 kbar).

pressure is shown in Fig. 16. The dependences of the lattice parameters on variables are different from one another in cases (1), (2), and (3) as follows:

Case (1): a-axis decreases, c-axis slightly increases, and volume decreases with increasing of pressure;

Case (2): a-axis increases, c-axis decreases, and volume increases with x;

Case (3): a-axis, c-axis, and volume decrease with increasing x.

It is to be noted that the addition of Ti^{3+} results in the increase of the volume.

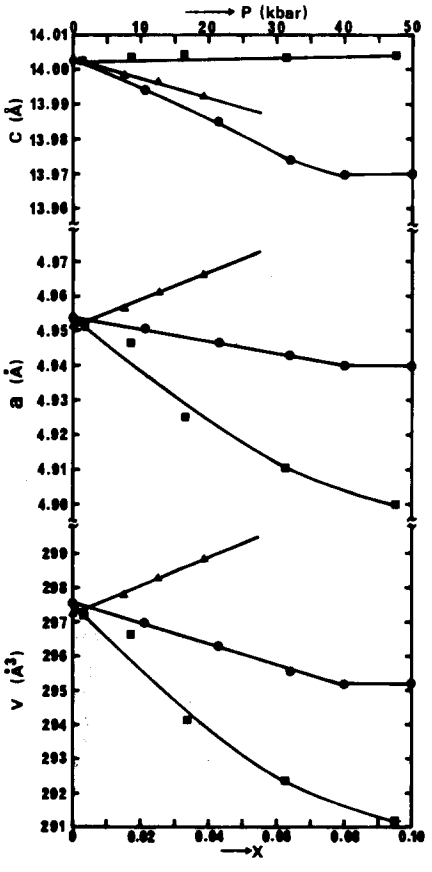

FIG. 16. Comparison of the lattice parameters vs composition x or pressure for V_2O_{3+x}, $(V_{1-x}Ti_x)_2O_3$, and pressured V_2O_3. The solid circles represent V_2O_{3+x} from present work, the solid triangles $(V_{1-x}Ti_x)_2O_3$ from Ref. (*3*), and the solid squares pressured V_2O_3 from Ref. (*2*).

Accordingly, it seems that the scaling between the addition of Ti and a positive pressure does not make sense for the volume. As the volume of the insulating phase is larger than that of the metallic phase in V_2O_3, it is reasonable that the pressure stabilizes the metallic phase. V_2O_3 is an insulator above T_{t2} and below T_{t1}, and the temperature dependences of the a-axis and c-axis in the intermediate metallic phase differ from each other, i.e., the a-axis dilates and the c-axis contracts with temperature. McWhan *et al.* (*3*) suggested that the itinerant to localized transition at T_{t2} is primarily in the e^T band, which then induces localization in the a^T band, where the a^T band is associated with the bonding orbitals along the c-axis and the e^T band is associated with orbitals which lie in the c-plane (*29*). This interpretation is consistent with the dilating of the a-axis and then the expansion in V–V distance in the plane when the temperature increases. This implies that the dilation of the a-axis with temperature plays an important role in the PM–PI transition at T_{t2}.

Next, let us show that the dilation of the c-axis with decreasing temperature is closely related to the PM–AFI transition at T_{t1}. Figure 3 shows the temperature dependence of the lattice parameters of nonstoichiometric V_2O_{3+x}. In all samples, the a-axis smoothly decreases and the c-axis increases almost linearly with decreasing temperature. The samples with $x = 0.00$ and 0.020 show the metal–insulator transition at about 160 and 80°K, respectively, and the length of the c-axis just before the transition is almost equal in both samples and the value is about 14.012 Å. On the other hand, the samples with $x = 0.045$ and 0.062 show no metal–insulator transition and the length of the c-axis, interpolated to $T = 0$, is much shorter than 14.012 Å. These results suggest the existence of critical length of the c-axis below which the alloy system remains entirely metallic.

In the system $(V_{1-x}Ti_x)_2O_3$, the c-axis decreases with increasing of the composition x, and therefore the above-mentioned interpretation can be applied to the system. McWhan *et al.* (*3*) reported that the coefficient of thermal expansion (α) of the c-axis at 298°K is -5.6×10^{-6}/°K for the sample with $x=0.04$ in $(V_{1-x}Ti_x)_2O_3$. We tried to estimate the temperature change of the c-axis for the samples $x=0.04$ and 0.055 using the length of the c-axis of each sample at 298°K and α, assuming that α is almost independent of the temperature and the composition x. The results are shown by the broken line in Fig. 3. The calculated line for the $x=0.04$ sample reaches to the critical line at about 60°K and for the $x=0.055$ sample does not reach to the critical line even at zero. This predicts that the $x=0.04$ sample shows the PM–AFI transition at about 60°K and the composition $x=0.055$ is almost the critical composition above which the alloy system remains entirely metallic. The prediction is consistent with the observed results in the $(V_{1-x}Ti_x)_2O_3$ system. Thus, we found out that the decrease of T_{t1} with x in the V_2O_{3+x} and $(V_{1-x}Ti_x)_2O_3$ systems is closely connected with the c-axis decrement with x, which is a common character in both systems, and moreover there is a critical length of the c-axis ($\simeq$14.01 Å) below which the compound remains metallic.

In case (1), the c-axis slightly increases with pressure but nevertheless the metal–insulator transition is suppressed with increasing pressure. It is very difficult to state the reason for this result, because there is no data on the temperature dependence of lattice parameters under pressure.

In the $(V_{1-x}Cr_x)_2O_3$ system, the addition of Cr^{3+} causes a rise in the resistivity of the metallic phase and the addition of Ti or nonstoichiometry does not greatly affect the electric property of the metallic phase. Therefore it is likely that another more significant factor on the PM–AFI transition may exist in the system $(V_{1-x}Cr_x)_2O_3$. However, the system related to V_2O_3 shows the PM–AFI transition when the c-axis crosses over a critical value, at least in V_2O_{3+x}.

Acknowledgments

The authors are grateful to Professor T. Takada and Dr. S. Muranaka for offering a chance to use the torquemeter. We also thank Professor T. Shinjo, Professor H. Yasuoka, and Professor J. B. Goodenough for helpful discussions.

References

1. A. MENTH, A. C. GOSSARD, AND J. P. REMEIKA, *J. Phys.* (*Paris*) C **1**, 1107 (1971).
2. D. B. MCWHAN AND J. P. REMEIKA, *Phys. Rev.* B **2**, 3734 (1970).
3. D. B. MCWHAN, A. MENTH, J. P. REMEIKA, W. F. BRINKMAN, AND T. M. RICE, *Phys. Rev. B* **7**, 1920 (1973).
4. D. B. MCWHAN, T. M. RICE, AND J. P. REMEIKA, *Phys. Rev. Lett.* **23**, 1384 (1969).
5. A. JAYARAMAN, D. B. MCWHAN, J. P. REMEIKA, AND P. D. DERNIER, *Phys. Rev. B* **2**, 3751 (1970).
6. N. F. MOTT, *Proc. Phys. Soc. London* **62**, 416 (1949); *Phil. Mag.* **6**, 287 (1961).
7. N. F. MOTT, *J. Phys.* (*Paris*) **32**, C1-11 (1971).
8. R. I. BEECROFT AND A. SWENSON, *J. Phys. Chem. Solids* **15**, 234 (1960).
9. A. JAYARAMAN, *Phys. Rev.* **137**, A179 (1965).
10. T. KATSURA AND M. HASEGAWA, *Bull. Chem. Soc. Japan* **40**, 561 (1967).
11. M. NAKAHIRA, S. HORIUCHI, AND H. OOSHIMA, *J. Appl. Phys.* **41**, 836 (1970).
12. D. B. MCWHAN, A. MENTH, AND J. P. REMEIKA, *J. Phys.* (*Paris*) **31**, C-1079 (1971).
13. K. NAGASAWA, Y. BANDO, AND T. TAKADA, *J. Cryst. Growth* **17**, 143 (1972).
14. N. KIMIZUKA, M. ISHII, M. SAEKI, M. NAKANO, AND M. NAKAHIRA, *Solid State Commun.* **12**, 43 (1973).
15. J. C. LAUNAY, M. POUCHARD, AND R. AYROLES, *J. Cryst. Growth* **36**, 297 (1976).
16. Y. UEDA, K. KOSUGE, S. KACHI, T. SHINJO, AND T. TAKADA, *Mater. Res. Bull.* **12**, 87 (1977).
17. Y. UEDA, T. OHTANI, K. KOSUGE, AND S. KACHI, *Mater. Res. Bull.* **13**, 305 (1978).
18. E. D. JONES, *Phys. Rev.* **137**, A978 (1964).
19. A. C. GOSSARD, D. B. MCWHAN, AND J. P. REMEIKA, *Phys. Rev. B* **2**, 3762 (1970).

20. Y. UEDA, K. KOSUGE, S. KACHI, H. YASUOKA, H. NISHIHARA, AND A. HEIDEMANN, *J. Phys. Chem. Solids* **39**, 1281 (1978).
21. J. DUMAS AND C. SCHLENKER, *J. Magn. Mater.* **7**, 252 (1978).
22. Y. UEDA, K. KOSUGE, S. KACHI, AND T. TAKADA, *J. Phys. (Paris) C* **2**, 275 (1979).
23. K. NAGASAWA, Y. BANDO, AND T. TAKADA, *J. Appl. Phys.* **8**, 1262 (1969); **9**, 407 (1970).
24. K. KAWASHIMA, Y. UEDA, K. KOSUGE, AND S. KACHI, *J. Cryst. Growth* **26**, 321 (1974).
25. D. B. MCWHAN, J. P. REMEIKA, J. P. MAITA, H. OKINAKA, K. KOSUGE, AND S. KACHI, *Phys. Rev. B* **7**, 326 (1973).
26. A. C. GOSSARD, J. P. REMEIKA, T. M. RICE, H. YASUOKA, K. KOSUGE, AND S. KACHI, *Phys. Rev. B* **9**, 1230 (1974).
27. A. C. GOSSARD, F. J. DISALVO, L. S. ERICH, J. P. REMEIKA, H. YASUOKA, K. KOSUGE, AND S. KACHI, *Phys. Rev. B* **10**, 4178 (1974).
28. D. B. MCWHAN AND T. M. RICE, *Phys. Rev. Lett.* **22**, 887 (1969).
29. J. B. GOODENOUGH, *in* "Progress in Solid State Chemistry" (H. Reiss, Ed.), Vol. 5, p. 145, Pergamon, Elmsford, N.Y. (1971).
30. H. KÜWAMOTO, H. V. KEER, J. E. KEEM, S. A. SHIVASHANKAR, L. L. VAN ZANDT, AND J. M. HONIG, *J. Phys. (Paris) C* **4**, 35 (1976).